Hysteresis from antiferromagnet domain-wall processes in exchange-biased systems: Magnetic defects and thermal effects

Joo-Von Kim* and R. L. Stamps
School of Physics, M013, University of Western Australia, 35 Stirling Hwy., Crawley WA 6009, Australia
(Received 22 March 2004; revised manuscript received 9 August 2004; published 9 March 2005)

The partial domain-wall theory of exchange bias predicts bias field magnitudes and film thickness dependencies consistent with certain experimental systems. However, the theory does not account for the coercivity enhancement that accompanies the hysteresis loop shift in single domain materials. We show theoretically that the presence of an attractive domain-wall potential in the antiferromagnet, arising from magnetic impurities, for example, can provide an energy barrier for domain-wall processes that control the coercivity. Asymmetric hysteresis loops are observed and modifications to the angular dependence of exchange bias suggest a mechanism of rotational hysteresis in terms of wall pinning. Similar domain-wall processes are also seen at finite temperatures, where an analogous pinning arises from a displacement of the domain wall from the interface due to thermal fluctuations.

DOI: 10.1103/PhysRevB.71.094405 PACS number(s): 75.25.+z, 75.70.Cn, 75.50.Ee, 75.60.−d

I. INTRODUCTION

Exchange bias refers to the effective unidirectional anisotropy induced in a ferromagnet (F) exchange coupled to an antiferromagnet (AF). The anisotropy can be initiated by cooling the ferromagnet/antiferromagnet system through the Néel temperature in the presence of an applied field. While the bias effect has been successfully engineered as a pinning mechanism in magnetoelectronic devices, quantitative theories for the underlying physical processes governing the bias are still being sought. The magnetic properties of a ferromagnet in an exchange biased system exhibit some interesting features. (1) The hysteresis loop is displaced along the field direction by a quantity referred to as the bias field (H_{eb}), which can either be positive or negative. (2) The width of the hysteresis loop can be simultaneously increased with the loop shift. (3) Repeated traces of the hysteresis loop can yield different values of the bias field; this is known as the "training effect." (4) No absolute measure of the bias can be obtained; dynamic measurements such as ferromagnetic resonance, Brillouin light scattering and ac susceptibility can give different estimates of the unidirectional anisotropy. For recent reviews on the topic, the reader is referred to Refs. 1–5.

The minimum criterion for exchange bias is a uniaxial anisotropy in the antiferromagnet, which is subsequently transferred to the ferromagnet as a unidirectional anisotropy, to lowest order, by exchange coupling across the ferromagnet/antiferromagnet interface. Initial insight into the problem came from Meiklejohn and Bean,[6,7] who supposed that the uniaxial anisotropy is sufficiently large such that the antiferromagnetic spins are not perturbed by the motion of the ferromagnet magnetization. The bilinear form of the exchange coupling between the two layers then appears as a fixed effective field for the ferromagnet and a unidirectional anisotropy appears straightforwardly. However, estimates of the loop shift from this model are two orders of magnitude larger than values obtained in experiment.

A resolution for this discrepancy was proposed following the observation that deformations in the magnetic spin structure, such as the formation of partial or complete domain walls, have an energy cost that is more compatible with experimental bias fields. Such a wall structure can form in the ferromagnet,[8,9] antiferromagnet,[10–13] or through both, depending on the configuration that minimizes the energy. Strong experimental evidence for the existence of such a wall in single-crystal materials has recently been obtained.[14] For an ideal system (specifically one that is free from imperfections and at zero temperature), the partial domain-wall theory of exchange bias proposed by Mauri *et al.*[11] does not predict any changes to the coercivity in addition to the loop shift for uncompensated interfaces. In fact, for an isotropic ferromagnet the domain wall produces only a shifted reversible magnetization curve.[13] The enhanced coercive field observed in experiment has been suggested to arise from domain-wall pinning in the ferromagnet at centers created by the interface roughness.[15] Others have argued for processes in the antiferromagnet to be the cause, including wall pinning,[16] irreversible transitions of grains,[17] and interactions between grains.[18] This is consistent with other experimental[19,20] and theoretical work,[21,22] where the impact of spin dilution and anisotropy changes in the antiferromagnet on the hysteresis of exchange-biased systems has been studied.

In this paper, we present a theory of coercivity enhancement in the partial wall model of exchange bias for a single domain material with uncompensated interfaces. Irreversible transitions are made possible by an energy barrier arising from magnetic impurities in the antiferromagnet or thermal effects. The physics of the wall formation can be viewed as a two-state process, where the partial wall center is the parameter that can either be close to the interface or moderately delocalized in the bulk. Magnetic defects, such as local variations in the exchange or magnetocrystalline anisotropy energies, lead to an attractive potential for the domain wall that can pin the wall under suitable conditions. An analogous behavior is observed at finite temperatures, where the wall displaces away from the interface due to thermal fluctuations. This process may be viewed in terms of the action of a

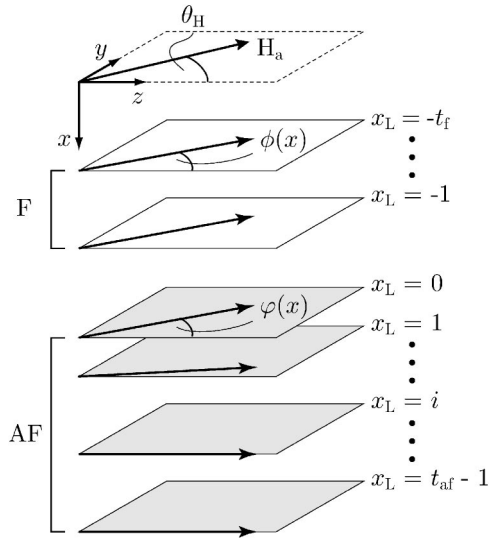

FIG. 1. Geometry of the ferromagnet/antiferromagnet bilayer. The ferromagnet occupies the space $-t_f \leqslant x_L \leqslant -1$ and the antiferromagnet occupies $0 \leqslant x_L \leqslant t_{af}-1$. The antiferromagnet easy axis is along the z direction, which serves as the reference for the layer-dependent angles ϕ and φ, and the applied field angle θ_H. Only one sublattice of the antiferromagnet is shown.

"virtual" pinning center in the antiferromagnet. In both cases, the transition between the two states is driven by the reversal of the ferromagnet to produce a shifted hysteresis loop.

The paper is organized as follows. Our model for the ferromagnet/antiferromagnet system is presented in Sec. II and the continuum limit of this model is studied in Sec. III, where we obtain some simple analytical expressions to describe the process of partial wall formation in the presence of magnetic impurities. In Sec. IV, we present numerical results of hysteresis calculations for a ferromagnet/antiferromagnet system with magnetic impurities in the antiferromagnet. The role of temperature is studied in Sec. V and concluding remarks are presented in Sec. VI.

II. MODEL

The ferromagnet/antiferromagnet bilayer is modeled as a simple-cubic lattice of localized spins, where the semiclassical limit is taken and each spin is represented by a vector $\mathbf{S}_i$, of constant length S, that may rotate freely in space. Translational invariance is assumed in the film plane and only uncompensated interfaces are considered. Thus, the antiferromagnet layer is treated as a series of ferromagnetic spin sheets with antiferromagnetic coupling between each layer perpendicular to the film plane. The magnetic configuration for the entire system is therefore completely specified by a chain of macroscopic spins S_i, where i labels the layer number. The bilayer geometry is shown in Fig. 1.

In addition to energy contributions from a static external magnetic field and magnetocrystalline anisotropy, each spin also interacts with its nearest neighbors through Heisenberg exchange. The local Hamiltonian for a spin at layer i is

$$\mathcal{H}_i = -\mu_0 \mathbf{H}_a \cdot (m_i \mathbf{S}_i) - \sum_j J_{ij} \mathbf{S}_i \cdot \mathbf{S}_j - K_i (\mathbf{S}_i \cdot \hat{\mathbf{z}})^2 + K_{\text{plane}} (\mathbf{S}_i \cdot \hat{\mathbf{x}})^2 \quad (1)$$

and is proportional to an energy per unit area, since the magnetization is taken to be uniform within each layer. The first term represents the interaction with an external magnetic field H_a, where μ_0 is the permeability of free space and m_i is the layer magnetic moment that takes on the value of m_f in the ferromagnet and m_{af} in the antiferromagnet. The second term represents the Heisenberg exchange between nearest-neighbor spins, where J_{ij} takes on the value of J_f in the ferromagnet, J_{af} in the antiferromagnet, and $J_{f\text{-}af}$ across the ferromagnet/antiferromagnet interface. The third term represents a uniaxial anisotropy energy in the antiferromagnet K_{af}, where the easy axis coincides with the z direction; the ferromagnet is taken to be isotropic. The last term is an easy-plane anisotropy that encourages planar rotation of the spins and approximates the magnetostatic fields generated by out-of-plane spin fluctuations. For future reference and unless specified otherwise, the parameters used throughout this paper are $J_f = 45.0$ meV, $J_{af} = J_{f\text{-}af} = -3.4$ meV, $K_{af} = 0.34$ meV/spin, $K_{\text{plane}} = 1.0$ meV/spin, and $m_f = m_{af} = 2.2\mu_B$/spin. The ferromagnet and antiferromagnet layers are each 20 monolayers thick ($t_f = t_{af} = 20$ML). The applied field is oriented at $\theta_H = 10°$ to minimize computation time. For a spin-1 system, the exchange parameters chosen give a Curie temperature (T_C) of 1043 K for the ferromagnet and a Néel temperature (T_N) of 79 K for the antiferromagnet. These transition temperatures are similar to those for a Fe/FeF_2 system but are chosen primarily so that $T_C \gg T_N$. We wish to stress that while specific material parameters have been used, our results could be applied to any composite material for which a partial wall mechanism leads to bias. Examples of such systems include ferromagnet/antiferromagnet structures with single-crystal antiferromagnetic insulators,[14] metallic antiferromagnets,[23] and exchange-spring systems.[24]

The calculated magnetization curve for the ferromagnet/antiferromagnet system defined above is shown in Fig. 2, with the corresponding spin structure at three values of the applied field. The details of the numerical procedure used is presented later in Sec. IV. At forward field ($h > 0$), the ferromagnet spins are completely aligned with the magnetic field, while the antiferromagnet spins are in a perfect Néel state, collinear with the easy axis, with the interface spin antiparallel to the ferromagnet due to the antiferromagnetic interlayer coupling. As the field is reduced and reversed, the anisotropy of the antiferromagnet pins the ferromagnet, through the interlayer coupling, along the positive direction until a critical value of the reverse field at which the magnetization begins to rotate. With the parameters used, the energy of a 180° Bloch wall in the antiferromagnet spin chain, $\sigma_{af} = 4\sqrt{J_{af} K_{af}/2} = 3.04$ meV, is less than the magnitude of the interlayer exchange. As such, it is more favorable energetically to deform the antiferromagnet spin structure during magnetization reversal than it is to "break" the interlayer coupling. This can be seen at points (ii) and (iii) in Fig. 2(b),

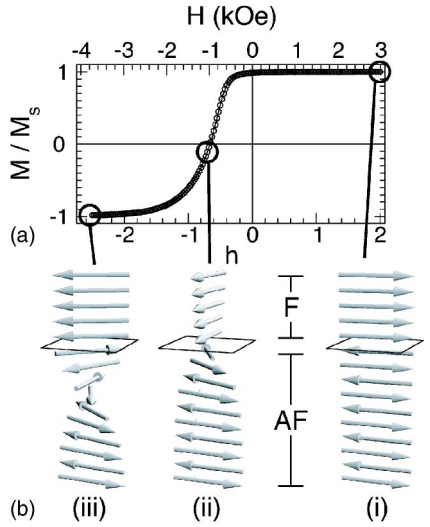

FIG. 2. (a) Magnetization curve for the ferromagnet/antiferromagnet system. (b) Calculated spin structure at three different points of the magnetization curve. The creation of a partial antiferromagnet domain wall can be seen in (iii). Only the spins close to the F/AF interface are shown. The reduced field unit h is defined in Eq. (2).

where a partial wall twists up as the ferromagnet rotates. The winding and unwinding of the partial wall is reversible, and because the ferromagnet is isotropic, the resulting magnetization curve is also reversible. Thus, partial-wall formation in antiferromagnet results in an additional energy cost for magnetization reversal and results in a displaced hysteresis loop, where the magnitude of the loop shift is proportional to the wall energy. It should be noted that this mechanism is only possible if the antiferromagnet film is sufficiently thick to support such a partial wall. With our parameters the theoretical Bloch wall width is $\lambda_{\mathrm{af}}=\pi\sqrt{J_{\mathrm{af}}/2K_{\mathrm{af}}}\simeq 7$ML, which is less than the film thickness, and defines a natural length scale for the antiferromagnet. The importance of pinning centers in the antiferromagnet would therefore depend not only on their strengths but also on their position relative to the interface (at distances comparable to λ_{af} from the interface). In this paper, we examine how the partial-wall mechanism is affected by the presence of defects in the antiferromagnet and by temperature.

The relevant scale for magnetic fields in this model is determined by the Zeeman energy of the ferromagnet and the antiferromagnet domain wall energy.[11,25] As such, it is convenient to express the external field H_a in terms of a reduced unit,

$$h=\frac{2\mu_0 H_a m_{\mathrm{f}} t_{\mathrm{f}}}{\sigma_{\mathrm{af}}}. \tag{2}$$

In the remainder of the paper, all applied field values will be expressed in terms of this reduced unit, which facilitates comparisons to other materials and ferromagnet film thicknesses, and in physical units (kA/m) with the material parameters given above.

III. CONTINUUM MODEL FOR DOMAIN-WALL PINNING

A simple physical picture of hysteresis from antiferromagnet domain-wall pinning can be obtained by taking the continuum limit of Eq. (1). To simplify the problem, the ferromagnet is approximated as a Stoner-Wohlfarth particle (uniform magnetization that rotates coherently in an external field), while deformations in the magnetic structure are permitted in the antiferromagnet. Closed-form solutions for the magnetic profile are obtained in the limit where the antiferromagnet staggered magnetization varies slowly compared to the lattice spacing in the direction perpendicular to the film plane. To treat the layer-to-layer variations in S_i in this continuum limit, we note that the antiferromagnet energy (where $\langle\cdots\rangle$ denotes a sum over nearest neighbors),

$$\mathcal{E}_{\mathrm{af}}=-\sum_{\langle i,j\rangle\in\mathrm{af}} J_{\mathrm{af}}\mathbf{S}_i\cdot\mathbf{S}_j-\sum_{i\in\mathrm{af}} K_{\mathrm{af}}(\mathbf{S}_i\cdot\hat{\mathbf{z}})^2, \tag{3}$$

remains invariant under the transformation

$$S_i=(-1)^i S_i' \quad (i\in\mathrm{af}) \tag{4}$$

if $J_{\mathrm{af}}<0$ is replaced by $|J_{\mathrm{af}}|$. It is further assumed the spin vectors are constrained to lie entirely in the yz plane, so the wall profile in the antiferromagnet can be described by a layer-dependent angle $\varphi(x)$ measured from the easy axis. The orientation of the ferromagnet is denoted by ϕ and the external field by θ_{H}. All angles described here are shown in Fig. 1. To be consistent with the transformation into staggered magnetization variables, we assume a ferromagnetic interlayer coupling in this discussion.

Following the treatment of wall pinning in ferromagnetic materials by Braun *et al.*,[26] we examine the influence of a pointlike impurity at an arbitrary position in the antiferromagnet. We suppose there is a small local variation in the uniaxial anisotropy at some distance $x_d>0$ from the interface,

$$K_{\mathrm{af}}'(x)=K_{\mathrm{af}}\left[1+\rho\delta\left(\frac{x-x_d}{\lambda_{\mathrm{af}}}\right)\right], \tag{5}$$

where ρ represents a fractional change in the anisotropy at the impurity. Neglecting the interlayer exchange, the energy of the partial wall in the antiferromagnet becomes

$$\mathcal{E}_{\mathrm{af}}[\varphi(x)]=\int_0^\infty dx\left[D_{\mathrm{af}}\left(\frac{\partial\varphi}{\partial x}\right)^2+K_{\mathrm{af}}'(x)\sin^2\varphi\right], \tag{6}$$

where $D_{\mathrm{af}}\equiv J_{\mathrm{af}}/(2a)$ is the antiferromagnet exchange stiffness and a is the lattice constant. Note that the integral is taken over a semi-infinite antiferromagnet, which is a valid approximation if the antiferromagnet film thickness is much larger than the domain-wall width. In the limit where the anisotropy fluctuation is small, deviations from the static Bloch wall profile due to the impurity can be neglected and a pinning energy,

$$\mathcal{E}_\rho=\rho K_{\mathrm{af}}\lambda_{\mathrm{af}}\,\mathrm{sech}^2\left(\frac{x_c-x_d}{\lambda_{\mathrm{af}}}\right), \tag{7}$$

can be obtained by substituting the standard domain-wall solution into the integral in Eq. (6). $\lambda_{\mathrm{af}}\equiv\sqrt{D_{\mathrm{af}}/K_{\mathrm{af}}}$ is the

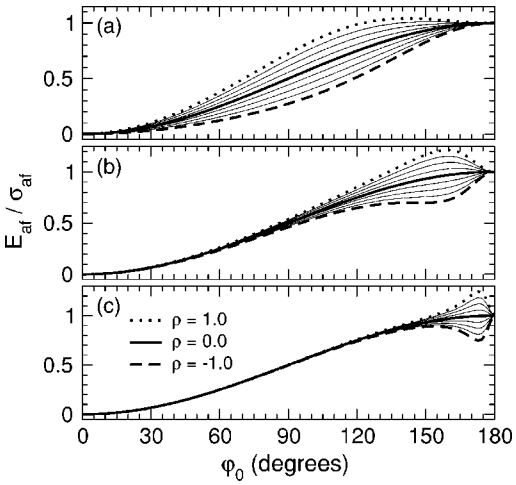

FIG. 3. Angular dependence of the partial-wall energy with point defects. The normalized antiferromagnet energy, $\mathcal{E}_{\rm af}(\varphi_0)/\sigma_{\rm af}$, is shown as a function of interface twist angle φ_0 for a series of impurity strengths, from $\rho=-1.0$ to 1.0 in increments of 0.2, and position: (a) $x_d/\lambda_{\rm af}=0.1\pi$, (b) $x_d/\lambda_{\rm af}=0.5\pi$, and (c) $x_d/\lambda_{\rm af}=0.9\pi$. An interface angle of $\varphi_0=180°$ corresponds to the formation of a 180° Bloch wall. Defects located beyond half a domain-wall width from the interface play no role in wall formation.

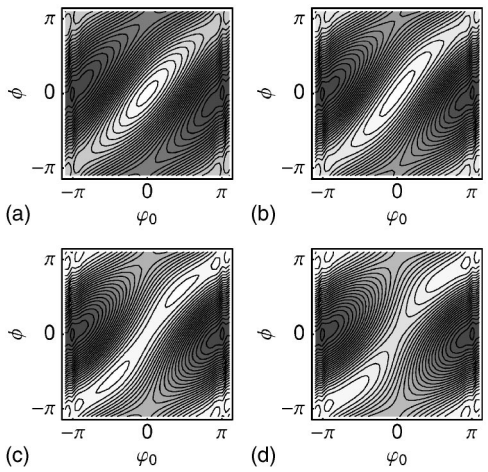

FIG. 4. Energy contour plot for the reversal of the ferromagnet in an applied field. The total energy is shown as a function of the orientation of the interface antiferromagnet spin φ_0 and the ferromagnet magnetization ϕ for a range of applied fields with $\theta_{\rm H}=0$: (a) $h=0$, (b) $h=-0.5$, (c) $h=-1.0$, and (d) $h=-1.5$. The lightest regions correspond to the lowest energy.

characteristic magnetic length in the antiferromagnet and x_c denotes the position of the wall center [i.e., $\varphi(x_c)=\pi/2$]. It is useful to express the energies in terms of the interface angle $\varphi_0\equiv\varphi(x=0)$, which is related to the wall center x_c from the expression for the Bloch wall profile,

$$x_c=\lambda_{\rm af}\ln\tan\left(\frac{\varphi_0}{2}\right). \tag{8}$$

The antiferromagnet energy can then be expressed entirely as a function of φ_0,

$$\mathcal{E}_{\rm af}(\varphi_0)=\frac{1}{2}\sigma_{\rm af}(1-\cos\varphi_0)+\frac{\rho K_{\rm af}\lambda_{\rm af}\sin^2\varphi_0}{\left(\cosh\frac{x_d}{\lambda_{\rm af}}+\cos\varphi_0\sinh\frac{x_d}{\lambda_{\rm af}}\right)^2}, \tag{9}$$

where $\sigma_{\rm af}\equiv 4\sqrt{D_{\rm af}K_{\rm af}}$ is the energy for a 180° antiferromagnetic Bloch domain wall. This function is sketched in Fig. 3 for different defect concentrations ρ.

Defects that decrease the anisotropy locally ($\rho<0$) lead to an overall reduction in the antiferromagnet energy. However, this reduction also gives rise to a local energy minimum for certain defect positions relative to the interface. Some examples are given in Fig. 3. As discussed previously, the reversal of the ferromagnet drags the antiferromagnet along with it, forming a partial wall. The lag angle $\phi-\varphi_0$ is only zero in the limit of strong interlayer coupling, so, in general, the twist formed is not a full 180° Bloch wall. Because the wall energy is largely concentrated at the center where the magnetization gradients are largest, centering the wall at x_d places these gradients in a local anisotropy minimum and so reduces the overall wall energy. As such, the wall becomes pinned when $x_c=x_d$, which corresponds to the value of φ_0 for which the local energy minimum appears. Defects located farther than half a domain-wall width from the interface (i.e., $x_d/\lambda_{\rm af}=\pi$) do not affect the twist formation, because the wall needs to de-pin completely from the interface in order to center about the impurity.

The depth of the energy well is governed by the magnitude of the local variation in $K_{\rm af}$. The position of the defect, relative to the interface, determines the width of the energy well measured in terms of φ_0. Close to the interface the pinning potential causes a broad local energy minimum, because an energy saving can be obtained by situating any gradient in the wall profile about the defect. For pinning sites located farther away the energy well becomes narrower, approaching a zero width as x_c gets close to half a wall width from the interface. No effects are seen for defects situated farther than half a domain-wall width from the interface. For impurities that enhance the local anisotropy ($\rho>0$) an energy barrier to domain-wall formation occurs instead.

To see how such defects can generate hysteresis in the ferromagnet, we consider the total energy of the bilayer,

$$\mathcal{E}_{\rm tot}=-\overline{B}H_a\cos(\theta_{\rm H}-\phi)-J_{\text{f-af}}\cos(\phi-\varphi_0)+\mathcal{E}_{\rm af}(\varphi_0), \tag{10}$$

where for convenience we have defined $\overline{B}\equiv\mu_0 m_{\rm f} t_{\rm f}$. The evolution of this energy with applied field is shown in Fig. 4 as a contour plot, with the interface antiferromagnet spin orientation shown on the horizontal axis and the ferromagnet orientation shown on the vertical axis. We consider a $\rho=-0.5$ defect located at $x_d/\lambda_{\rm af}=0.75\pi$. At forward and zero field there is only one minimum in the energy landscape, which corresponds to the untwisted case $\phi=\varphi_0=0$. As the field is reversed ($H_a<0$), the energy well corresponding to the minimum begins to widen, until a critical field is reached at which the ferromagnet magnetization begins to rotate and the partial twist in the antiferromagnet is wound up. At this point

a local minimum appears close to $(\varphi_0 = \pm\pi, \phi = \pm\pi)$ in which the partial wall can become trapped during reversal of the ferromagnet. As the field is increased for remagnetization, it is possible for the wall to remain trapped in this local minimum, even if this does not represent the lowest-energy state. Thus, the reversal process (a)→(b)→(c)→(d) in Fig. 4 may differ from the remagnetization process (d)→(c)→(b)→(a), leading to hysteretic behavior.

These results can be generalized to describe variations in the local exchange [connecting the magnetization at $\varphi(x)$ and $\varphi(x+\delta x)$, for example] under the same assumption that deviations from the static Bloch wall profile can be neglected. For a Bloch wall, the anisotropy energy $K_{\rm af}\sin^2[\varphi(x)]$ is equal to the exchange energy $D_{\rm af}(\partial_x\varphi(x))^2$ at any part along the wall.[68] Therefore, the point defect term introduced into the anisotropy can equally represent a local variation in the exchange bond,

$$D'_{\rm af}\left(\frac{\partial\varphi}{\partial x}\right)^2 = K'_{\rm af}\sin^2(\varphi), \tag{11}$$

which generates a pinning term proportional to $\mathrm{sech}^2(x)$ that is similar to Eq. (7).

IV. MAGNETIC DEFECTS

In order to treat pinning potentials of arbitrary strength, a numerical approach is used to determine the equilibrium spin configuration at arbitrary fields. As before, we assume translational invariance in the film plane but allow nonuniform configurations to develop along the direction perpendicular to the film. This is an approximation for a partial wall formed in a single grain. With the local spin Hamiltonian given by Eq. (1), the time evolution of each spin is calculated using the Landau-Lifshitz equation of motion

$$\frac{\partial\mathbf{S}_i}{\partial t} = -\gamma\mathbf{S}_i\times\mathbf{H}_i^{\rm eff} - \alpha\mathbf{S}_i\times(\mathbf{S}_i\times\mathbf{H}_i^{\rm eff}), \tag{12}$$

where γ is the gyromagnetic constant and α is a phenomenological damping constant. The effective field at each site $\mathbf{H}_i^{\rm eff}$ is given by the gradient in the energy with respect to the local spin variables,

$$\mathbf{H}_i^{\rm eff} = -\frac{1}{\mu_0 m_i}\nabla_{\mathbf{S}_i}\mathcal{E}_i. \tag{13}$$

For each hysteresis loop calculation, the initial state of the bilayer consists of a uniform ferromagnet aligned along the z axis with the antiferromagnet in a perfect Néel state collinear with the easy axis. At each field increment, the ground state is found self-consistently by integrating the coupled set of nonlinear differential equations described by Eq. (12). The new configuration then serves as the starting point for the next field increment. A combination of single-step (fourth-order Runge-Kutta) and multistep (predictor-corrector) time-integration methods is used. The Runge-Kutta scheme is employed primarily for difficult regions of phase space where large changes to the spin configuration take place, such as twist formation during reversal, for example. When changes to the spin orientations are small, such as in forward field where deviations from the initial state are small, it is possible to obtain solutions much faster with the predictor-corrector method (see Ref. 27, for example).

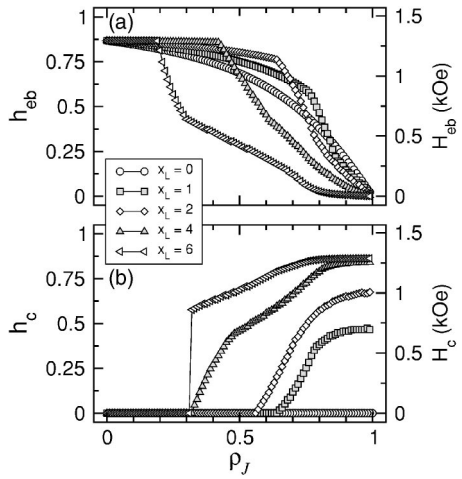

FIG. 5. Bias field and coercivity variations for reduced-exchange defects. (a) Bias field h_{eb} and (b) coercivity h_c are shown as functions of defect strength $\rho_J \equiv 1 - J_d/J_{\rm af}$ for a series of defect positions x_L in the antiferromagnet, where $x_L = 0$ corresponds to the interface layer and $x_L = t_{\rm af} - 1$ the free surface. The reduced field unit h is defined in Eq. (2).

Imperfections in the antiferromagnet are treated as local variations in the exchange or anisotropy constants. The effects of reduced exchange are shown in Fig. 5, where the bias field and coercivity are shown as functions of defect density. In our notation, a defect situated at x_L modifies the exchange coupling between layers $x_L - 1$ and x_L, i.e., $J_{\rm af}(x_L - 1, x_L) = J_d$, where $x_L = 0$ denotes the interface antiferromagnet layer. The reduction in the modified coupling is described by a defect strength $\rho_J \equiv 1 - J_d/J_{\rm af}$, which represents an average across the layer. Interfacial defects ($x_L = 0$) cause the bias field to decrease because the interlayer exchange coupling is reduced. As shown elsewhere the bias field is proportional to the interlayer coupling $J_{\text{f-af}}$ when $J_{\text{f-af}} \ll \sigma_{\rm af}$, but is largely independent of $J_{\text{f-af}}$ in the opposite limit $J_{\text{f-af}} \gg \sigma_{\rm af}$.[11,25,28] This behavior is reflected in the smooth decay of the bias field with defect concentration. For defects in the bulk of the antiferromagnet ($x_L > 0$), the reduction in the bias field arises from two sources. First, the reduction in the exchange coupling leads to an overall decrease in the partial-wall energy since $\sigma_{\rm af} \sim \sqrt{J_{\rm af}K_{\rm af}}$. Second, the defect can trap the partial wall in a local energy well as it is formed, giving rise to an energy barrier for depinning during remagnetization as argued in Sec. III. This leads to irreversible behavior and a nonzero coercivity accompanying the loop shift is indeed observed. The results in Fig. 5(a) indicate that the second process is more important in determining H_{eb}. For example, the bias field for a defect situated at $x_L = 6$ undergoes a rapid decay as the concentration is increased and reaches half its initial value at $\rho_J \simeq 0.3$, in contrast to the larger density required ($\rho_J \simeq 0.75$) to reduce H_{eb} by the same amount for a defect at $x_L = 2$.

Defects that modify the local anisotropy have a more modest effect on the hysteresis properties, as shown in Fig.

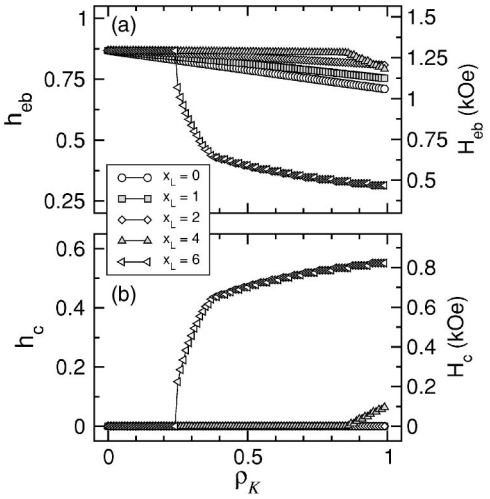

FIG. 6. Bias field and coercivity variations for reduced-anisotropy defects. (a) Bias field h_{eb} and (b) coercivity h_c are shown as functions of defect strength $\rho_K \equiv 1 - K_d/K_{\mathrm{af}}$ for a series of defect positions x_L in the antiferromagnet, where $x_L = 0$ corresponds to the interface layer and $x_L = t_{\mathrm{af}} - 1$ the free surface. The reduced field unit h is defined in Eq. (2).

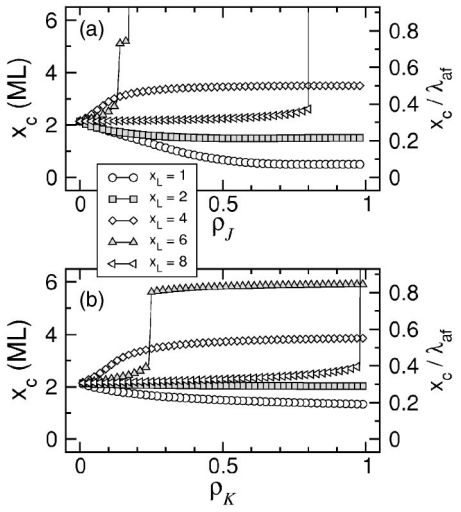

FIG. 7. Variation in the position of partial-wall center with magnetic defects. The antiferromagnet wall center x_c is shown as a function of defect density for (a) reduced-exchange and (b) reduced-anisotropy defects for a series of defect positions x_L, where $x_L = 0$ corresponds to the interface layer and $x_L = t_{\mathrm{af}} - 1$ is the free surface. Note that ρ_J defects denoted by x_L modify the exchange between the layers at $x_L - 1$ and x_L. The antiferromagnet wall width is $\lambda_{\mathrm{af}} \simeq 7$ML.

6. For defects close to the interface, changes to the bias field are comparatively small and are governed primarily by the reduction in the total wall energy arising from the local anisotropy variation. The pinning potential generated by such defects has a weak effect on the domain wall, as evidenced by the small increase in the coercivity at large defect concentration. Strong pinning of the partial wall is obtained for defects farther from the interface (e.g., $x_L = 6$ in Fig. 6), where a large coercive field accompanying a reduced bias field is observed for moderate to high defect concentrations. Such contrasting behavior between exchange and anisotropy defects is not captured by our analytical model presented earlier, because deformations to the Bloch wall profile were not taken into account. In contrast to exchange defects, variations in the local anisotropy do not disconnect two regions of the antiferromagnet but only create an attractive potential in which the partial wall can become pinned. The more dramatic changes in the hysteresis properties for exchange defects arise from the significant deformations induced in the wall profile.[29]

Defect-induced domain-wall pinning is clearly illustrated in Fig. 7, where the position of the wall center is shown as a function of defect density for exchange and anisotropy defects. The values of the wall center position x_c shown are taken at maximum reverse field in a hysteresis loop trace, corresponding to the point at which the extent of the partial wall formed is greatest. The attraction of the wall to the pinning center can be seen as the wall center drifts away from the zero-density value $x_{c0} \simeq 2$ toward x_L with increasing defect concentration. Recall that an exchange defect denoted by x_L refers to a modified coupling between layers x_L and $x_L - 1$, which means the corresponding defect position is actually $x_L - 0.5$. Defects close to the interface move the wall center closer to the antiferromagnet. Farther into the bulk, the pinning potential can cause a complete detachment of the partial wall from the interface. These processes are indicated by the sharp transitions for $x_L = 6$ and $x_L = 8$ in Fig. 7(a), and $x_L = 8$ in Fig. 7(b). In these cases the bias is suppressed completely and a large coercivity is obtained.

Irreversible rotations of the ferromagnet, due to a combination of wall pinning and depinning transitions, give rise to asymmetric hysteresis loops. Some examples are given in Fig. 8. The loops are calculated with an exchange defect at $x_L = 5$ for three different values of ρ_J. At low defect concentrations, the pinning potential is insufficient to modify

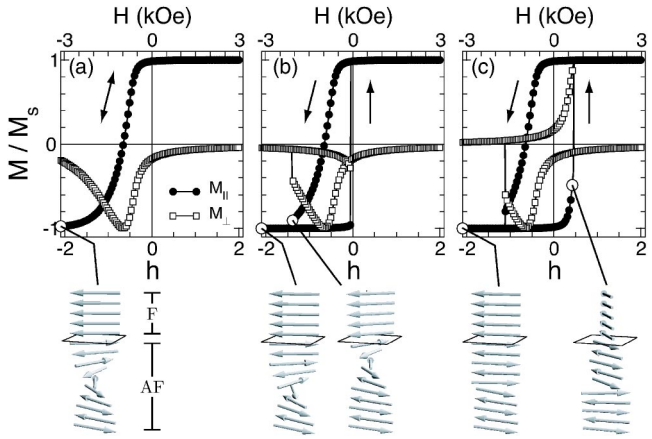

FIG. 8. Defect-induced asymmetry in hysteresis loops. The hysteresis loops are shown for a reduced exchange defect at $x_L = 5$ for three concentrations: (a) $\rho_J = 0.15$, (b) $\rho_J = 0.45$, and (c) $\rho_J = 0.75$. The components of magnetization parallel ($M_{\parallel}$) and perpendicular ($M_{\perp}$) to the field direction are shown. The arrows indicate the directions for reversal and remagnetization. The reduced field unit h is defined in Eq. (2). The spin configuration near the interface is shown for selected field values below the hysteresis curves.

partial-wall formation. The resulting magnetization curve, as shown in Fig. 8(a), is reversible and resembles the curve obtained with the absence of impurities. Pinning of the partial wall occurs during reversal for moderate concentrations, which appears as a sharp rotation of the magnetization at negative fields, as shown in Fig. 8(b). During remagnetization the wall is released from the pinning center at a different field, thus resulting in an asymmetry in the hysteresis loop. The release of the wall is indicated by a sharp transition in M. The energy barrier between wall pinning and release increases with defect concentration, resulting in a larger coercivity and reduced bias [Fig. 8(c)].

The rotation sense of the ferromagnet is influenced by the strength of the pinning potential. This dependence can be seen from the evolution of component of magnetization perpendicular to the field direction, $M_{\perp}$, throughout the hysteresis loop trace. Reversal is executed with a clockwise rotation for the three defect concentrations considered, as indicated by the negative values of $M_{\perp}$ along the path toward negative field. For weak pinning ($\rho_J=0.15$) the remagnetization into forward field is executed with an unwinding of the partial wall in a counterclockwise direction, where twisting of the wall is unhindered by the defect. At moderate defect concentrations ($\rho_J=0.45$), the magnetization process again takes place with a counterclockwise rotation, however, the motion in this case consists of a fast depinning of the wall from the defect. For defects that cause large reductions in the local exchange coupling, the width of the domain wall can be reduced to a single lattice spacing, where most of the entire spatial magnetization gradient is centered about the defect. This is the case in Fig. 8(c), where the magnetization profiles shown after reversal bear evidence of this reduction in wall width. In this scenario, winding up the twist further does not cost more energy and remagnetization can proceed with the same sense of rotation (i.e., clockwise).

The pinning potentials are only effective within a certain angular range of the applied field, which can be seen in the angular dependence of the bias field and coercivity. Some examples are given for reduced-exchange defects in Fig. 9. Reductions in the interlayer coupling, produced by interface defects ($x_L=0$), result in a decrease in the bias field across the entire range of applied field angles [Fig. 9(a)]. This behavior is consistent with the continuum theory developed previously, where the bias field dependence on $J_{\text{f-af}}$ enters in a straightforward way.[25] Because no frustration is introduced by the interfacial defects considered here, in contrast to rough interfaces,[25,29] there is no change in the natural angle of the ferromagnet (the equilibrium orientation of the ferromagnet in the absence of any applied fields). For defects located farther into the bulk, the angular dependence can be modified significantly. Outside of an angular range $\Delta\theta_H$ measured about the hard axis of the antiferromagnet [shown for $\rho_J=0.9$ in Fig. 9(c)] the bias field is observed to be largely suppressed and accompanied by an enhanced coercivity [Figs. 9(b) and 9(c)]. Inside this angular range the hysteresis properties do not appear to be modified by the defect and all curves are degenerate with the zero-concentration curve.

The angular range $\Delta\theta_H$ defines a "passive region" in which bias is not modified by the defect. In this region, the wall center does not reach sufficiently close to the defect to be affected by the pinning potential. The resulting hysteresis loops are therefore similar to the zero-concentration case, where the partial wall can wind and unwind unhindered to give a reversible magnetization curve. Defect-induced wall pinning is possible outside of the passive region, where the energy barrier imposed by the pinning potential largely determines the hysteresis properties. The size of the passive region depends on the position and magnitude of the pinning potential.

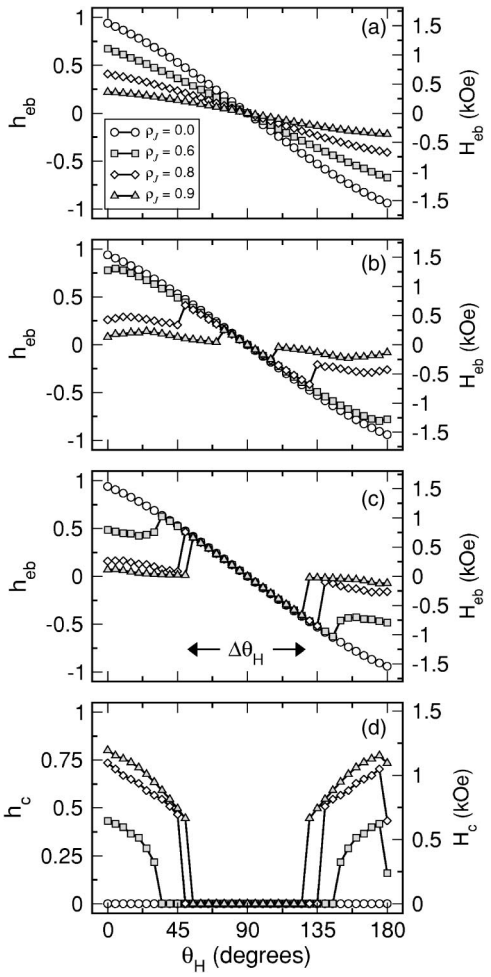

FIG. 9. Defect-modified angular dependence of exchange bias. The bias field h_{eb} is shown as functions of the applied field orientation θ_H, for a series of reduced-exchange defect positions: (a) $x_L=0$, (b) $x_L=2$, (c) $x_L=4$. The coercivity h_c is shown in (d) for the corresponding curves in (c). The reduced field unit h is defined in Eq. (2).

Domain-wall pinning close to the interface is a possible mechanism for exchange bias in thin antiferromagnet films. In the absence of impurity pinning, the angular range over which reversible twisting of the AF partial wall can occur is shown in Fig. 10(a) for a series of AF film thicknesses (cf., Fig. 4 in Ref. 13). Here, we plot the energy of an isolated AF film, normalized to the 180° Bloch wall energy, as a function of the spin orientation at one surface of the film. This mimics the dragging of the interface AF spin by the reversal of the F layer in the exchange biased bilayer (cf., Fig. 3). For thin films ($t_{\text{af}}=2,4$ML) the energy curves are symmetric about

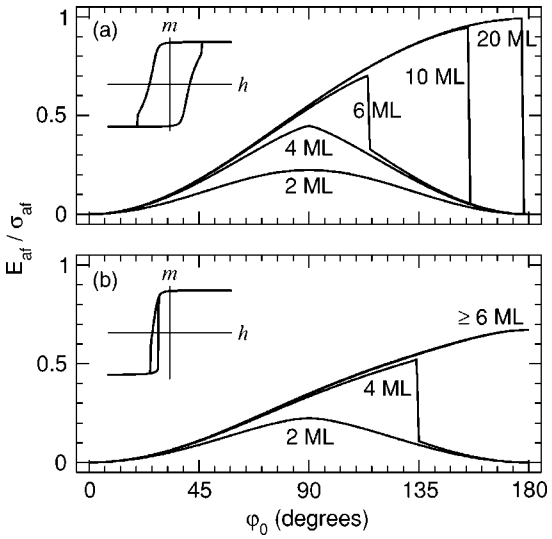

FIG. 10. Reversible and irreversible rotations of the partial antiferromagnet wall. The normalized antiferromagnet energy $\mathcal{E}_{\rm af}/\sigma_{\rm af}$ is shown as a function of twist angle φ_0 for different antiferromagnet film thicknesses with (a) zero defects and (b) $\rho_J=0.7$ reduced-exchange defect at $x_L=1$. Inset: schematic of the corresponding hysteresis loop for $t_{\rm af}=6$ML.

the hard axis direction ($\varphi_0=90°$) and show no irreversible transitions. In this regime, the end AF spin drags all the other AF spins along with it in unison, so only the uniaxial anisotropy $K_{\rm af}$ is sampled. The symmetry about the hard axis direction is broken for thicker films ($t_{\rm af}\geqslant 6$ML), where a high-energy branch appears as a partial twist is wound up following the rotation of the end AF spin away from $\varphi_0=0°$ through $\varphi_0=90°$. Past a critical angle, an irreversible transition to the low-energy branch is made as the twist is wound off the other end of the AF film. This critical angle is strongly dependent on the AF film thickness and approaches 180° in the limit of a semi-infinite AF slab. This behavior is in stark contrast to the defect-modified system. An example is given in Fig. 10(b), where a reduced-exchange defect with $\rho_J=0.7$ at $x_L=1$ can be seen to stabilize the twist over the entire angular range $0°\leqslant\varphi_0\leqslant 180°$ for AF films as thin as 6ML. (Recall that the theoretical Bloch wall width is $\lambda_{\rm af}\simeq 7$ML in the absence of defects). To illustrate this point further, hysteresis loops for the $t_{\rm af}=6$ML system are shown as insets for the zero-defect and the exchange-defect cases in Fig. 10. For the zero-defect case, the hysteresis loop is symmetric with a large coercivity resulting from the antiferromagnet uniaxial anisotropy, while a shifted asymmetric loop is observed in the defect-modified system. As such, defect-induced pinning can account for bias in antiferromagnets thinner than the Bloch wall width, as observed in a number of experimental systems.[20,30–38]

V. FINITE TEMPERATURE EFFECTS

Recent theoretical work has demonstrated that a loss of bias can occur due to thermal fluctuations that destabilize the partial antiferromagnet wall at elevated temperatures close to the Néel temperature.[39] We show here that such processes share similar features with defect-induced wall pinning. At finite temperatures, the analogous pinning potential occurs through spatial variations of effective local fields, which are due to thermal fluctuations in a uniform spin configuration. Temperature is incorporated into our numerical model with a local mean-field theory, where the thermally averaged magnetic moment $\langle S\rangle$ of each spin is calculated self-consistently using[40]

$$\langle S\rangle = S_0 B\left(\frac{\mu_0 m\mathbf{S}\cdot\langle\mathbf{H}^{\rm eff}\rangle}{k_B T}\right), \tag{14}$$

where S_0 is the spin magnitude at zero temperature, B is the Brillouin function, and $\langle\cdots\rangle$ denotes a thermal average. The effective field $\langle\mathbf{H}^{\rm eff}\rangle$ at layer i becomes

$$\langle\mathbf{H}_i^{\rm eff}\rangle = \mathbf{H}_a + \sum_j \frac{J_{ij}}{\mu_0 m_j}\langle\mathbf{S}_j\rangle + \frac{2K_i}{\mu_0 m_i}\langle\mathbf{S}_i\rangle. \tag{15}$$

The ground state and thermal averages are solved self-consistently with the same numerical scheme presented earlier.

Before discussing the effects of finite temperatures on the exchange bias system, it is useful to examine first the thermal properties of an isolated antiferromagnet domain wall. Here, we follow the approach of Papanicolaou for computing the spin structure of an isolated antiferromagnet Bloch wall in a one-dimensional spin chain.[41] We consider a chain of 100 spins whose initial configuration consists of a two domain state. In the first half of the chain, the spins are in a Néel state where the first spin points up ($+z$) and the last spin points down ($-z$). The second half of the chain is also in a Néel state, except that the first spin points down and the last spin points up. The profile for the domain wall separating the two regions can be obtained by allowing this configuration to come to equilibrium using the numerical procedures described earlier. We apply this method to study the wall structure at different temperatures and for antiferromagnets with different anisotropy constants (i.e., to give a range of domain wall widths). Spatial variations in the thermal averaged moment $\langle S\rangle$ are shown in Fig. 11. The curves are arranged such that $x_L=0$ corresponds to the center of the domain wall. The interesting feature common to all anisotropy values considered is the sharp reduction in $\langle S(x)\rangle$ at the center of the domain wall. Because the gradient in the spin orientation is largest at the wall center, the effective field acting on the center spin is reduced by the mean-field averaging. This is a compounding effect as a reduction in the effective field leads to a further reduction in $\langle S\rangle$. Magnetization gradients at the wall center are greater for narrower walls, which consequently lead to large reductions in $\langle S\rangle$, as seen in Figs. 11(c) and 11(d). The profile of the domain wall is not observed to deform significantly as the temperature is varied, which indicates that an additional reduction in wall energy occurs through the spatial variation in $\langle S(x)\rangle$. As we shall show shortly, the reduction in $\langle S(x)\rangle$ at the wall center plays the role of a virtual defect for thermal wall pinning. The difference here is that the analogous defect potential is a result of thermal fluctuations in the wall structure itself.

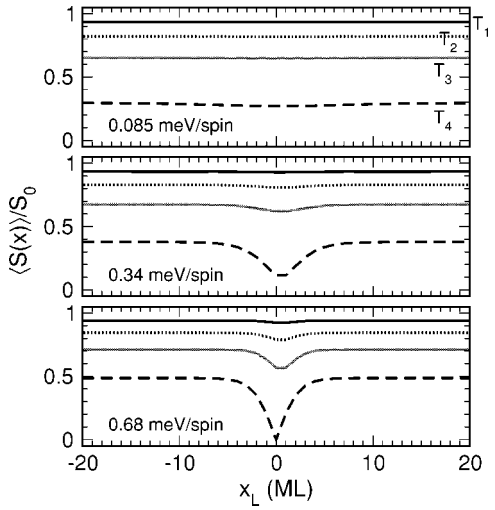

FIG. 11. Thermally averaged spin profile for antiferromagnetic domain wall. $\langle S\rangle$, as a function of position along the antiferromagnet with a 180° Bloch wall, is shown for a series of temperatures: $T_1=10$ K, $T_2=30$ K, $T_3=50$ K, and $T_4=70$ K ($T_N=79$ K). The variations are shown for three values of the antiferromagnet anisotropy K_{af}.

The temperature dependence of the bias field and coercivity are shown in Fig. 12 for three values of K_{af}. The results are obtained from a series of calculated hysteresis loops taken at different temperatures. The bias field is observed to decrease monotonically as temperature increases and to vanish below the Néel temperature (79 K) close to $T\simeq 70$ K for the three cases considered. Within the same temperature range in which the bias decreases rapidly, one observes a nonzero coercive field accompanying the loop shift. The magnitude of the coercivity enhancement is also observed to be proportional the stiffness of the domain wall, where the largest increase in h_c is seen for $K_{\mathrm{af}}=0.68$ meV/spin and the smallest increase for $K_{\mathrm{af}}=0.085$ meV/spin. This suggests that the irreversible behavior is driven by a domain wall process, where the energy barriers that facilitate the irreversible transitions are governed by the wall energy in some way. The coercivity peaks at the Blocking temperature, where the bias vanishes, and then continues to decrease monotonically for higher temperatures.

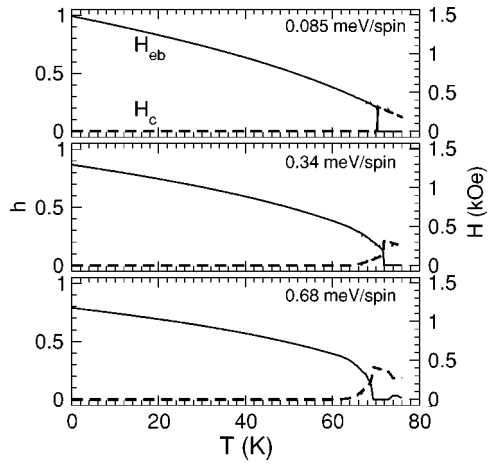

FIG. 12. Temperature dependence of exchange bias. Bias field H_{eb} and coercivity H_c are shown as functions of temperature T for three values of K_{af}. The reduced field unit h is defined in Eq. (2).

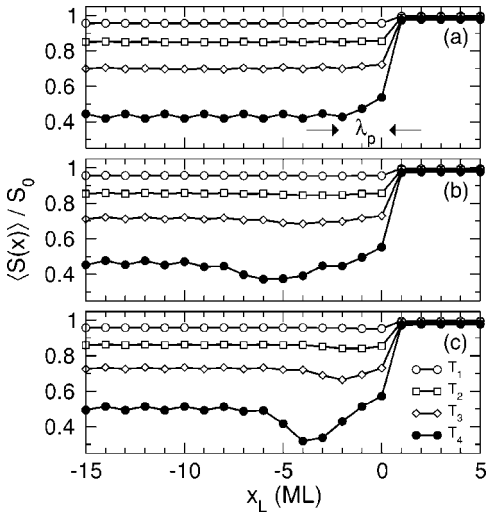

FIG. 13. Thermal magnetization profile of the ferromagnet/antiferromagnet bilayer. The spatial variation of $\langle S\rangle$ is shown at (a) forward field for $K_{\mathrm{af}}=0.085$ meV/spin, (b) maximum reverse field for $K_{\mathrm{af}}=0.085$ meV/spin, and (c) maximum reverse field for $K_{\mathrm{af}}=0.34$ meV/spin. The curves are shown for four different temperatures: $T_1=10$ K, $T_2=30$ K, $T_3=50$ K, and $T_4=70$ K. The interface layer of the antiferromagnet is situated at $x=0$ and the antiferromagnet occupies the region $-t_{\mathrm{af}}-1\leqslant x\leqslant 0$. In (a) the penetration length of the ferromagnet λ_p is shown for T_4.

This peak in the coercive field has been reported for a few experimental systems[42–44] and has been attributed to the rearrangement of magnetic domains at the critical temperature. We argue here that thermal wall processes similar to defect-induced pinning can account for such hysteretic behavior close to the Néel temperature. Consider the spatial profile $\langle S(x)\rangle$ for the ferromagnet/antiferromagnet bilayer presented in Fig. 13 for two K_{af} cases. At forward field [Fig. 13(a)], the antiferromagnet is in a Néel state. The thermal magnitude of the antiferromagnet spins decreases sharply from the interface and attains a constant average value throughout the remainder of the film. A larger $\langle S\rangle$ is present at the interface due to the stabilizing effect of the ferromagnet layer, whose ordering temperature is an order of magnitude larger than the Néel temperature. The decay of $\langle S\rangle$ from the interface to the bulk is characterized by a penetration length λ_p, which is temperature dependent and is a measure of how strongly the ferromagnet spins influence the antiferromagnet moments located farther away from the interface. λ_p is indicated for $T_4=70$ K in Fig. 13(a). A sawtooth pattern develops in $\langle S\rangle$ and is a result of the external field, which lifts the degeneracy between the sublattice spins (i.e., the Zeeman interaction favors spins oriented parallel to the applied field). At reverse field the partial wall profile can be seen superimposed on the spatial variation of $\langle S\rangle$ [Figs. 13(b) and 13(c)]. A sharp dip corresponding to the wall center is observed, which becomes more pronounced at high temperatures. For both antiferromagnets considered the wall center shifts away from the in-

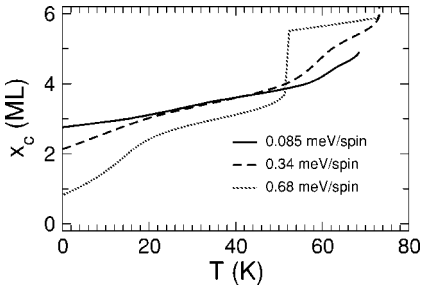

FIG. 14. Variation of partial antiferromagnet wall center with temperature. The wall center x_c at maximum reverse field in a hysteresis loop is shown as a function of temperature T for three values of the antiferromagnet anisotropy K_{af}.

terface as the temperature at which the hysteresis loop is performed is increased. This is particularly evident for the stiffer antiferromagnet with $K_{\mathrm{af}}=0.68$ meV/spin [Fig. 13(c)]. One observes that the wall center x_c at maximum negative field moves from $x_L \approx 2$ at $T_3=50$ K to $x_L \approx 4$ at $T_4=70$ K. This represents a significant change in the wall position with temperature, given that the wall width is $\lambda_{\mathrm{af}} \simeq 5$ML for $K_{\mathrm{af}}=0.68$ meV/spin.

The displacement of the partial wall from the interface at elevated temperatures can be understood as follows. A Bloch domain wall has the largest energy density at the wall center at which the spatial magnetization gradient is the steepest. At finite temperatures, it is more favorable energetically to position the wall center in a region in which $\langle S \rangle$ is reduced. As such, the spatial decay in $\langle S \rangle$ at the interface, into the antiferromagnet, "repels" the wall center as the partial twist is formed and results in a weak depinning of the wall from the interface. This depinning transition cannot occur unless the spatial extent of the dip at the wall center is narrower than λ_p, and that the natural position of the wall center (i.e., x_c at 0 K) is comparable to λ_p. In light of our earlier results on defect-modified bias, this thermal wall process can be likened to pinning by a virtual defect in the antiferromagnet. Here, the position and strength of the virtual defect is strongly temperature dependent, which can be seen in the temperature dependence of the wall center (measured at maximum reverse field) as shown in Fig. 14. The wall is observed to shift away from the interface as the temperature for each loop measurement is increased. For a large range of temperatures below T_N the wall center remains within λ_p of the interface, which means that the partial wall can be wound and unwound reversibly to give a bias loop shift with zero coercivity. The discontinuity in $x_c(T)$ at higher temperatures indicates a depinning of the wall from the interface, giving rise to an irreversible process analogous to defect-induced pinning.

The angular dependence of exchange bias at elevated temperatures is also modified by such thermally driven virtual pinning processes. An example is given in Fig. 15, where the bias field and coercivity are shown as a function of the applied field angle for the three K_{af} cases considered previously. For the weaker anisotropy material [Fig. 15(a)] the angular variation of the exchange bias does not depart significantly from the zero-temperature sinusoidal behavior,

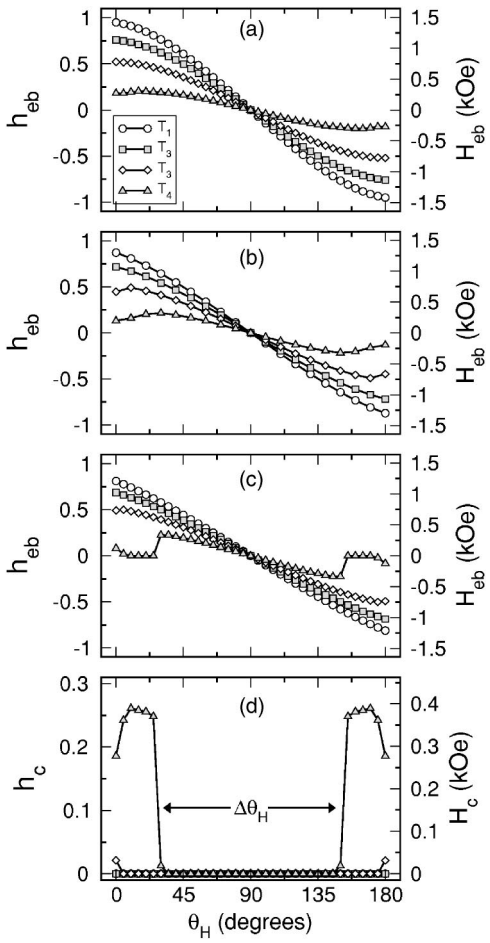

FIG. 15. Angular dependence of exchange bias at finite temperatures. The bias field h_{eb} as a function of applied field angle θ_{H} is shown for three different antiferromagnet anisotropy values K_{af}: (a) 0.085 meV/spin, (b) 0.34 meV/spin, and (c) 0.68 meV/spin. The angular variation in the coercivity h_c for $K_{\mathrm{af}}=0.34$ meV/spin is given in (d). The angular variations are presented for four temperatures: $T_1=10$ K, $T_2=30$ K, $T_3=50$ K, and $T_4=70$ K ($T_N=79$ K). The reduced field unit h is defined in Eq. (2).

where the bias maximum coincides with an applied field along the easy axis direction. A uniform decrease in the bias field at all angles is observed with increasing temperature. For larger anisotropies [Figs. 15(b) and 15(c)] the bias field maximum shifts away from the easy axis direction, for example, from $\theta_{\mathrm{H}}=0$ to $\theta_{\mathrm{H}} \approx 10°$ at $T=50$ K and to $\theta_{\mathrm{H}} \approx 30°$ at $T=70$ K in Fig. 15(b) with corresponding shifts in the bias minimum. A more dramatic effect is seen for $K_{\mathrm{af}}=0.68$ meV/spin close to the Blocking temperature, where the bias disappears completely for a range of applied field angles about the easy axis [Fig. 15(c)]. These features share many similarities with the defect-modified angular dependence discussed earlier. For thermal-induced "pinning" there is an analogous passive region $\Delta\theta_{\mathrm{H}}$, shown for $K_{\mathrm{af}}=0.68$ meV/spin at $T=70$ K in Fig. 15(d), in which the hysteresis is not modified. Outside the passive region a large enhancement in the coercivity with a vanishing loop shift is observed.

The position and strength of the virtual pinning potential is determined by two competing length scales. First, the de-

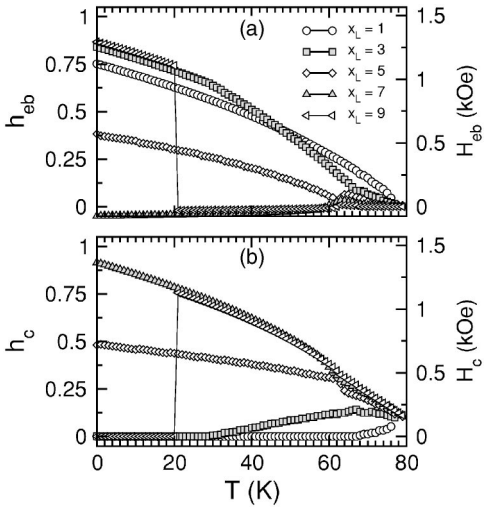

FIG. 16. Defect-enhanced thermal pinning of domain wall. (a) Bias field h_{eb} and (b) coercivity h_c as functions of temperature T for a series of exchange-defect positions x_L, for $\rho_J=0.5$. The reduced field unit h is defined in Eq. (2).

cay length λ_p characterizing the spatial variation in $\langle S\rangle$ at the interface is governed by the relative magnitudes of the Curie and Néel temperatures. Second, the antiferromagnet domain-wall width is determined by the antiferromagnet exchange and anisotropy energies. As discussed above, thermal-induced wall pinning is important when the two length scales are comparable, i.e., for cases where the position of the partial wall center at $T=0$ K is within λ_p of the interface. For an antiferromagnet with defects, one might expect correlations between the thermal- and impurity-induced wall pinning. Some examples are shown in Fig. 16, where the thermal dependence of exchange bias is shown with a reduced-exchange defect ($\rho_J=0.5$) in the antiferromagnet. Within a penetration depth λ_p of the interface the defects do not affect the hysteresis properties ($x_L \geqslant 1$), which is evidenced by a uniform decrease in the bias field accompanied by a small coercivity close to T_N is observed. The proximity of the defect to the interface does not allow it to function effectively as a pinning center, particularly at higher temperatures, because the thermal magnitude $\langle S\rangle$ is relatively large within the penetration region and the reduction in the exchange is insufficient to counter the influence of the ferromagnet. Evidence of a correlation between the thermal and impurity pinning can be seen for moderate to large defect distances from the interface ($x_L \geqslant 3$), where the temperature range over which nonzero coercive fields appear become broader.

VI. DISCUSSION AND CONCLUDING REMARKS

The reduction in the bias field induced by the defects is consistent with ion-irradiation experiments on exchange biased NiFe/FeMn systems,[45,46] where it was observed that bias can be controlled by varying the dose of the incoming ions. Other studies have shown an enhancement in the bias field can be obtained using the same experimental technique.[47,48] It is possible to account for the observed increase in the bias with the present model by increasing the local anisotropy, equivalent to a repulsive defect potential. Physically, structural changes leading to strain-related enhancements in the anisotropy have been shown to be possible.[49–52] This has been explored in more detail elsewhere.[21] However, recent experimental evidence suggests that irradiation of the ferromagnetic layer is essential for bias enhancement.[46] This is beyond the scope of this paper.

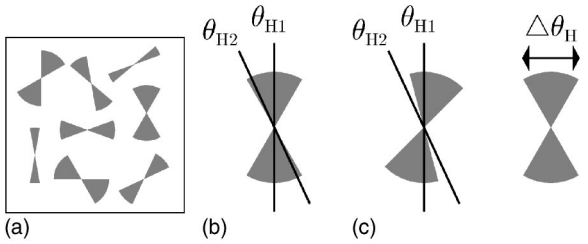

FIG. 17. Model of rotational hysteresis. $\Delta\theta_H$ represents the passive region associated with a particular defect. (a) An ensemble of antiferromagnet grains with defects gives rise to a distribution of passive regions withvarying amplitude and orientation. (b) Rotations of the magnetic field (e.g., $\theta_{H1}\leftrightarrow\theta_{H2}$) within passive regions lead to reversible winding or unwinding of the partial wall. (c) Rotations that cross the boundary of a passive region lead to irreversible depinning transitions of the partial wall.

Asymmetric hysteresis loops have been measured in a number of experimental systems.[16,53–64] In certain cases, complementary polarized neutron reflectometry experiments have shown that these observations can be explained by a reversal via coherent rotation and a remagnetization process involving domain-wall propagation.[54] Krivorotov *et al.* explained asymmetric hysteresis in their Fe/MnF_2 system with a threefold anisotropy term,[59] but the results in this section instead offer an interpretation in terms of domain-wall pinning processes in the antiferromagnet. This explanation is consistent with some recent work of Nikitenko *et al.* on the NiFe/FeMn system,[53] who concluded the presence of an antiferromagnet wall at the interface is necessary to explain their hysteresis measurements.

An interpretation of rotational hysteresis can be made in light of these results. In real materials, one may suppose that a large number of pinning sites in the antiferromagnet, of different magnitudes and distances from the interface, can give rise to an ensemble of passive regions (where wall pinning does not occur), as depicted in Fig. 17(a). Furthermore, for an ensemble of grains at the interface, the easy axis direction may vary from grain to grain so the orientation of these passive regions need not be collinear. Let θ_{H1} denote the field orientation at an arbitrary point in a rotational hysteresis experiment. Supposing that the ferromagnet is uniform, an ensemble of partial twists is formed in the antiferromagnet with magnitudes determined by the relative orientation of the local easy direction and θ_{H1}. Suppose that the field is now rotated by a small amount to θ_{H2}. If the new ferromagnet orientation remains within the passive region of a given grain, then the rotation causes the partial wall in the grain to wind or unwind slightly, which is a reversible process [Fig. 17(b)]. However, if a transition is made across the

boundary of a passive region the partial twist in the corresponding grain may be depinned from the interface due to the local defect [Fig. 17(c)]. This is an irreversible process. Hence, the extent of the partial walls formed and the number of depinning transitions depend on the history of the rotation. For example, the rotation of the field from θ_{H2} to θ_{H1} would not necessarily produce the same results, because the configuration of partial twists at θ_{H2} may not lead to the same initial state at θ_{H1}. This asymmetry between the two sense of rotation gives rise to rotational hysteresis.

We have dealt exclusively with a one-dimensional spin chain in our model. This is an approximation for an antiferromagnet grain with an uncompensated interface, where only one sublattice is in contact with the ferromagnet. Thus, assuming that the magnetization is uniform within a layer, the variations in spin orientation can be treated with a one-dimensional model. The average reduction in J_d would represent an average over a particular layer in a real system. Such control over defect placement could be achieved in a synthetic antiferromagnet, where a nonuniform thickness in the spacer layer would achieve a variation in the exchange coupling. Experiments involving the substitution of nonmagnetic atoms would also produce candidate structures, where defect placement is controlled by selective introduction of the nonmagnetic species.

Temperature has been included in our model using a local mean-field theory, which completely neglects any thermal fluctuations in the spin orientation. This approach was employed to obtain a qualitative picture of the thermal dependence of bias. Close to the Néel temperature fluctuations due to thermal magnons would test the stability of the wall structure in the antiferromagnet. The in-plane anisotropy would then act as an energy barrier to the reversal of the wall, leading to a finite probability with which the thermal excitations could destroy the wall completely. This has been investigated in more detail elsewhere.[39,65–67]

In summary, we have investigated the impact of magnetic impurities and temperature on the formation of an antiferromagnet partial domain wall in an exchange-biased system. Attractive potentials created by magnetic defects are shown to cause a depinning transition of the partial wall that leads to coercivity enhancement. Similarly, an analogous process is shown to arise from thermal effects close to the ordering temperature of the antiferromagnet. A reduction in the blocking temperature is also observed.

ACKNOWLEDGMENTS

The authors would like to thank L. Wee, R. E. Camley, P. N. Loxley, D. Suess, and T. Mewes for stimulating discussions. This work was supported by the Australian Research Council.

*Present address Institut d'Electronique Fondamentale, UMR CNRS 8622, Université Paris-Sud, 91405 Orsay cedex, France. Electronic address: joo-von.kim@ief.u-psud.fr

[1] J. Nogués and I. K. Schuller, J. Magn. Magn. Mater. **192**, 203 (1999).
[2] A. E. Berkowitz and K. Takano, J. Magn. Magn. Mater. **200**, 552 (1999).
[3] R. L. Stamps, J. Phys. D **33**, R247 (2000).
[4] M. Kiwi, J. Magn. Magn. Mater. **234**, 584 (2001).
[5] C. Binek, *Ising-type Antiferromagnets: Model Systems in Statistical Physics and in the Magnetism of Exchange Bias* (Springer-Verlag, Berlin, 2003).
[6] W. H. Meiklejohn and C. P. Bean, Phys. Rev. **102**, 1413 (1956).
[7] W. H. Meiklejohn and C. P. Bean, Phys. Rev. **105**, 904 (1957).
[8] M. Kiwi, J. Mejía-López, R. D. Portugal, and R. Ramírez, Europhys. Lett. **48**, 573 (1999).
[9] M. Kiwi, J. Mejía-López, R. D. Portugal, and R. Ramírez, Appl. Phys. Lett. **75**, 3995 (1999).
[10] L. Néel, Ann. Phys. (Paris) **2**, 61 (1967).
[11] D. Mauri, H. C. Siegmann, P. S. Bagus, and E. Kay, J. Appl. Phys. **62**, 3047 (1987).
[12] A. P. Malozemoff, Phys. Rev. B **35**, 3679 (1987).
[13] N. C. Koon, Phys. Rev. Lett. **78**, 4865 (1997).
[14] A. Scholl, M. Liberati, E. Arenholz, H. Ohldag, and J. Stohr, Phys. Rev. Lett. **92**, 247201 (2004).
[15] C. Leighton, J. Nogués, B. Jönsson-Åkerman, and I. K. Schuller, Phys. Rev. Lett. **84**, 3466 (2000).
[16] V. I. Nikitenko, V. S. Gornakov, L. M. Dedukh, Y. P. Kabanov, A. F. Khapikov, A. J. Shapiro, R. D. Shull, A. Chaiken, and R. P. Michel, Phys. Rev. B **57**, R8111 (1998).
[17] M. D. Stiles and R. D. McMichael, Phys. Rev. B **63**, 064405 (2001).
[18] H. Fujiwara, K. Zhang, T. Kai, and T. Zhao, J. Magn. Magn. Mater. **235**, 319 (2001).
[19] P. Miltényi, M. Gierlings, J. Keller, B. Beschoten, G. Güntherodt, U. Nowak, and K. D. Usadel, Phys. Rev. Lett. **84**, 4224 (2000).
[20] J. Keller, P. Miltényi, B. Beschoten, G. Güntherodt, U. Nowak, and K. D. Usadel, Phys. Rev. B **66**, 014431 (2002).
[21] J.-V. Kim and R. L. Stamps, Appl. Phys. Lett. **79**, 2785 (2001).
[22] U. Nowak, K. D. Usadel, J. Keller, P. Miltényi, B. Beschoten, and G. Güntherodt, Phys. Rev. B **66**, 014430 (2002).
[23] F. Y. Yang and C. L. Chien, Phys. Rev. Lett. **85**, 2597 (2000).
[24] S. Mangin, F. Montaigne, and A. Schuhl, Phys. Rev. B **68**, 140404 (2003).
[25] J.-V. Kim, R. L. Stamps, B. V. McGrath, and R. E. Camley, Phys. Rev. B **61**, 8888 (2000).
[26] H.-B. Braun, J. Kyriakidis, and D. Loss, Phys. Rev. B **56**, 8129 (1997).
[27] D. P. Landau and M. Krech, J. Phys.: Condens. Matter **11**, R179 (1999).
[28] J. Geshev, Phys. Rev. B **62**, 5627 (2000).
[29] J.-V. Kim, Ph.D. thesis, University of Western Australia, 2002.
[30] P. J. van der Zaag, R. M. Wolf, A. R. Ball, C. Bordel, L. F. Feiner, and R. Jungblut, J. Magn. Magn. Mater. **148**, 346 (1995).
[31] T. Ambrose and C. L. Chien, J. Appl. Phys. **83**, 6822 (1998).
[32] D. V. Dimitrov, S. Zhang, J. Q. Xiao, G. C. Hadjipanayis, and C. Prados, Phys. Rev. B **58**, 12090 (1998).
[33] H. Sang, Y. W. Du, and C. L. Chien, J. Appl. Phys. **85**, 4931

(1999).
[34] J. van Driel, F. R. de Boer, K.-M. H. Lenssen, and R. Coehoorn, J. Appl. Phys. **88**, 975 (2000).
[35] H. Y. Li, L. Y. Chen, and S. M. Zhou, J. Appl. Phys. **91**, 2243 (2002).
[36] B. Beschoten, J. Keller, P. Miltényi, and G. Güntherodt, J. Magn. Magn. Mater. **240**, 248 (2002).
[37] B. Negulescu, L. Thomas, Y. Dumont, M. Tessier, N. Keller, and M. Guyot, J. Magn. Magn. Mater. **242–245**, 529 (2002).
[38] M. Ali, C. H. Marrows, and B. J. Hickey, Phys. Rev. B **67**, 172405 (2003).
[39] L. Wee, R. L. Stamps, and R. E. Camley, J. Appl. Phys. **89**, 6913 (2001).
[40] D. L. Mills, Phys. Rev. B **3**, 3887 (1971).
[41] N. Papanicolaou, Phys. Rev. B **51**, 15062 (1995).
[42] C. Schlenker, Phys. Status Solidi **28**, 507 (1968).
[43] E. Fulcomer and S. H. Charap, J. Appl. Phys. **43**, 4184 (1972).
[44] C. Hou, H. Fujiwara, K. Zhang, A. Tanaka, and Y. Shimizu, Phys. Rev. B **63**, 024411 (2001).
[45] T. Mewes, R. Lopusnik, J. Fassbender, B. Hillebrands, M. Jung, D. Engel, A. Ehresmann, and H. Schmoranzer, Appl. Phys. Lett. **76**, 1057 (2000).
[46] S. Poppe, J. Fassbender, and B. Hillebrands, Europhys. Lett. **66**, 430 (2004).
[47] A. Mougin, T. Mewes, M. Jung, D. Engel, A. Ehresmann, H. Schmoranzer, J. Fassbender, and B. Hillebrands, Phys. Rev. B **63**, 060409 (2001).
[48] J. Juraszek, J. Fassbender, S. Poppe, T. Mewes, B. Hillebrands, D. Engel, A. Kronenberger, A. Ehresmann, and H. Schmoranzer, J. Appl. Phys. **91**, 6896 (2002).
[49] L. Néel, J. Phys. Radium **15**, 225 (1954).
[50] J. G. Gay and R. Richter, Phys. Rev. Lett. **56**, 2728 (1986).
[51] P. Bruno, J. Phys. F: Met. Phys. **18**, 1291 (1988).
[52] C. H. Lee, H. He, F. J. Lamelas, W. Vavra, C. Uher, and R. Clarke, Phys. Rev. B **42**, 1066 (1990).
[53] V. I. Nikitenko, V. S. Gornakov, A. J. Shapiro, R. D. Shull, K. Liu, S. M. Zhou, and C. L. Chien, Phys. Rev. Lett. **84**, 765 (2000).
[54] M. R. Fitzsimmons, P. Yashar, C. Leighton, I. K. Schuller, J. Nogués, C. F. Majkrzak, and J. A. Dura, Phys. Rev. Lett. **84**, 3986 (2000).
[55] C. Leighton, M. Song, J. Nogués, M. C. Cyrille, and I. K. Schuller, J. Appl. Phys. **88**, 344 (2000).
[56] C. Leighton and I. K. Schuller, Phys. Rev. B **63**, 174419 (2001).
[57] C. Leighton, M. R. Fitzsimmons, P. Yashar, A. Hoffmann, J. Nogués, J. Dura, C. F. Majkrzak, and I. K. Schuller, Phys. Rev. Lett. **86**, 4394 (2001).
[58] M. R. Fitzsimmons, C. Leighton, A. Hoffmann, P. C. Yashar, J. Nogués, K. Liu, C. F. Majkrzak, J. A. Dura, H. Fritzsche, and I. K. Schuller, Phys. Rev. B **64**, 104415 (2001).
[59] I. N. Krivorotov, C. Leighton, J. Nogués, I. K. Schuller, and E. D. Dahlberg, Phys. Rev. B **65**, 100402 (2002).
[60] M. Gierlings, M. J. Prandolini, H. Fritzsche, M. Gruyters, and D. Riegel, Phys. Rev. B **65**, 092407 (2002).
[61] I. Panagiotopoulos, N. Moutis, and C. Christides, Phys. Rev. B **65**, 132407 (2002).
[62] F. Radu, M. Etzkorn, T. Schmitte, R. Siebrecht, A. Schreyer, K. Westerholt, and H. Zabel, J. Magn. Magn. Mater. **240**, 251 (2002).
[63] M. Gierlings, M. J. Prandolini, M. Gruyters, W. D. Brewer, and D. Riegel, J. Magn. Magn. Mater. **240**, 280 (2002).
[64] D. Spenato, S. P. Pogossian, and H. L. Gall, J. Magn. Magn. Mater. **262**, 294 (2003).
[65] R. L. Stamps, Phys. Rev. B **61**, 12174 (2000).
[66] R. L. Stamps and L. Wee, IEEE Trans. Magn. **36**, 3170 (2000).
[67] L. Wee, Ph.D. thesis, University of Western Australia, 2002.
[68] This is a general property of solitons, where a dispersive component is always counterbalanced by another term that tends to diminish the spatial spread of the profile.